Process Safety and Environmental Protection, Volume 153, September 2021, pp. 439-451
DOI:10.1016/j.psep.2021.07.038

EXPERIMENTAL STUDY OF ACCIDENTAL LEAKAGE BEHAVIOUR OF LIQUID CO_2 UNDER SHIPPING CONDITIONS

Hisham Al Baroudi, Kumar Patchigolla, Dhinesh Thanganadar, Kranthi Jonnalagadda

Centre for Thermal Energy Systems and Materials (CTEM), School of Water, Energy and Environment (SWEE), Cranfield University, Cranfield, Bedfordshire, MK43 0AL, U.K.

*corresponding author e-mail address: k.patchigolla@cranfield.ac.uk

Nomenclature

u	Flow velocity (m/s)
f	Fanning factor
d	Pipe diameter (m)
Re	Reynolds Number
ŋ	Molecular viscosity (kg/m^{-1} s^{-1})
α	Vapour fraction
μ_{JT}	Joule Thomson coefficient (K MPa^{-1})
h	Specific enthalpy (kJ kg^{-1})
Y	Vapour/solid split fraction
O	Orifice size (mm)
d_e	Diameter of the source (mm)
C	Concentration value (mol%)
k	Linear correlation constant
x	Downstream distance (mm)

Subscript

1	initial
2	final
g	gaseous
s	solid
gs	Difference between sold and gaseous

Abstract

CO_2 shipping is a viable transport alternative when pipelines are impractical. Lack of experience in large-scale CO_2 shipping projects implies uncertainty in selecting optimal cargo conditions and operational safety procedures. The risk of uncontrolled release of CO_2 arises in case of mechanical failure of storage or cargo vessels, and a thorough understanding of the discharge phenomena, including the propensity for solid formation, is necessary to develop safety protocols. A refrigerated experimental setup is established in this study to investigate the release phenomena of liquid CO_2 under shipping conditions. The rig features a dome-ended cylindrical pressure vessel, a discharge pipe section and a liquid nitrogen refrigeration system that enables conditioning near the triple point – at ~0.7 MPa, 223 K - and higher liquid pressures (~2.6 MPa, 263 K). Pressure, temperature and mass monitoring were considered to enable an extensive observation of the leakage behaviour under typical operation scenarios. Three different sets of experiments were considered to inform the designer in the selection of optimal process conditions, with low-pressure (0.7 – 0.94 MPa, 223 – 228 K), medium-pressure (1.34 – 1.67 MPa, 234 – 245 K) and high-pressure tests (1.83 – 2.65 MPa, 249 – 259 K) demonstrating distinct behaviours relative to phase transitions, leakage duration and solidification of inventory.

Keywords: GHG; CCUS; CO_2 transport; CO_2 shipping; operational safety; leakage

Introduction

In response to the global warming crisis experienced as a result of anthropogenic industrial activities, carbon capture, utilisation and storage (CCUS) has been identified as a key option to reduce atmospheric emissions of CO_2 [1]. This technology consists of three principal steps – nominally capture of CO_2 from anthropogenic emitters, its transmission to the sink and storage [2]. Pipelines and sea vessels have been identified as the principal means for large-scale CO_2 transportation [3–6], each exhibiting their techno-economic feasibilities in relation to different project variables [7–9]. Generally, CO_2 shipping is deemed advantageous to discharge relatively small volumes of carbon dioxide over long distances due to its flexibility in sink-source matching and low capital investment costs [10,11]. The selection of transport conditions of future CO_2 shipping for CCUS projects is still under debate with respect to techno-economic [12] and process safety considerations [13–15]. Refrigerated liquid conditions of CO_2 relevant to the shipping chain are broadly categorised into low-pressure and temperature conditions (0.6 – 1 MPa, 218 – 233 K), medium pressure and temperature conditions (1.5 – 1.9 MPa, 243 – 253 K) and high-pressure and temperature conditions (>1.9 MPa and 253 K) [13–15] in the literature. Process safety considerations are expected to have a profound impact on the choice of shipping conditions [16]. The propensity for operational issues such as material defects, mechanical failure which can result in cracks and loss of containment [17]. Previous studies focused on pipeline systems suggested that carbon dioxide can lead to a degradation of non-metallic components [18] which poses a serious threat to the integrity of the system. Accidental releases and leakages thus represent a hazard during sea vessel transportation of liquid CO_2 too, which could put humans, marine life and the carrier in danger due to oxygen displacement over a large area. A thorough understanding of leakage hazards and loss of containment scenarios of sea vessels is necessary for any successful commercial implementation of this technology and assurance of high levels of process safety and integrity throughout the chain. Releases in the liquid phase, and particularly in proximity of the triple point, are complex phenomena which involve phase transitions, dispersion of dense and gas phase inventory, solid CO_2 formation and pressure and temperature drops in the cargo vessel

[19,20]. The UK's Health and Safety Executive [21] highlighted that CO_2 releases in the refrigerated liquid state still require experimental validations of the developed discharge models to determine hazard distances and appropriate safety protocols to be adopted. Due to its density being higher than that of air, CO_2 tends to accumulate in depressed areas, creating a risk of asphyxiation to the surrounding environment. Han et al. [22] investigated the implementation of a jettisoning system that could promptly discharge liquid CO_2 inventory from a defected tank in case of mechanical rupture of the vessel to mitigate the potential danger compromising the safety of the crew and integrity of the carrier. Experiments showed that high-pressure liquid CO_2 undergoes two distinct phase changes (liquid to liquid-vapour/liquid-vapour and then solid-vapour) throughout the tube that represented the jettisoning line during the discharge, with phase changes taking place at different locations throughout the pipe. In a follow-up work [23], the authors moreover found that a ventilation system to be paired with the jettisoning discharge would provide an additional level of safety to the operators involved. Speed of the ship is here deemed to be a key factor, with low speed enhancing safety for passengers inside the ship during ventilation and high speeds being safer for general public outside the carrier during jettisoning [23]. Shafiq et al. [24] performed a simulation work of CO_2 depressurisation from a high-pressure vessel (4 MPa and 233 K) in relation to orifice sizes of 4.325 mm, 6.325 mm and 8.325 mm and found that risk of solidification and blockages during the blowdown process can be drastically reduced by selecting the smallest orifice diameter. In a following work, the authors [25] performed a modelling campaign and relative experimental validation to scrutinise dry ice formation during blowdown of CO_2-CH_4 mixture from a cryogenic distillation column at initial temperature of 243 K and pressure of 4 MPa. The authors moreover derived a correlation to determine the optimal blowdown orifice size to be adopted in case of an emergency occurrence as to eliminate the risk of inventory solidification whilst also promoting the fastest discharge times. Most of the available literature concerning CO_2 accidental release for carbon dioxide transport systems focuses under pipeline conditions. Liu et al. [26] investigated the flow behaviour and impact of high-pressure CO_2 (8 – 10 MPa) jet discharges with respect to different nozzle sizes (3 – 20 mm) and found that the effect of the released jet represents the main hazard in case of pipeline leakage. Gu et al. [27] performed an experimental campaign on a 14.9 m long pipeline with a 15 mm internal diameter to explore the accidental leakage behaviour of CO_2 under different conditions (5 – 8.5

MPa, 296 – 313 K). Attention was dedicated to the temperature characteristics under different initial phase states – namely gaseous, supercritical and liquid. The study showed that carbon dioxide under liquid state demonstrated a wider temperature drop envelope compared to gaseous and supercritical conditions. Addition of variable amounts of N_2 impurity (2 – 6 mol%) in the stream moreover affected the discharge behaviour of the inventory. Mocellin et al. [28] focused on a comprehensive approach that explored both experimental and model-based study of abrupt CO_2 expansion at pressures of 1.1 – 3.6 MPa and temperature of 293 K. Developed models demonstrate robust agreement with experimental findings in relation to predicted discharge time. However, for shipping conditions, when leakage occurs the liquid CO_2 quickly vaporises and expands, causing solid formation and thermal deformation. This has clearly safety implications that need to be understood in relation to its thermal characteristics depending on the leakage scenarios. Based on these characteristics it is possible to reduce the occurrence of leakages and consequently reduce the suffocation by workers exposed to high CO_2 concentrations and thus minimise the damage to environment/marine life. Work from Hébrard et al. [29] focused on releases of 300 kg CO_2 from a 5 m long pipeline with 50 mm internal diameter at high-pressure dense phase of approximately 5 MPa conditions; the authors found that full-bore releases result in a build-up of liquid outflow in the first transient stage, followed by a stable release and a second transient stage; following the phase transition in the section, vapour release is accompanied by a significant reduction in outflow, with the vessel dropping below the triple point and forming dry-ice in the last stage. Hulsbosch-Dam et al [30] performed vertical liquid CO_2 releases from a 1 L vessel at different pressures (6 - 18 MPa) and varying nozzle sizes - 6.4 and 12.7 mm – and found that initial pressure has a limited impact on duration of the release, with nozzle diameter exerting a larger influence. The authors highlighted that the vertical orientation of the leakage nozzle could have an impact on the amount of liquid CO_2 pushed through the opening and thus the speed of the exit jet. Pursell [31] explored liquid and gas phase releases of CO_2 at pressures between 4 – 5.5 MPa from a 60 L vessel. Xie et al. [32] explored the leakage behaviour of supercritical CO_2 releases at different pressures (5 MPa, 7 MPa and 8 MPa) and maximum temperature of 323 K in a pipeline featuring a 30 mm diameter and 23 m length. A highly under-expanded jet structure was observed in featuring smaller nozzle sizes (1 mm and 3 mm) with this structure disappearing with increased nozzle size of 5 mm. Discharges at higher pressures were found to

exhibit lower depressurisation rates and take longer to achieve complete blowdown of the system due to the effect of chocked flow at the exit. The work showed the increase of nozzle size contributed to shorter leakage durations. Tian et al [33] experimentally investigated the release behaviour from a high-pressurised CO_2 vessel in liquid and gaseous phase in relation to different rupture sizes (1 mm, 2 mm and 3 mm) and temperatures (293 K and 323 K) and found that the different states resulted in a distinctly different decompression process. Discharges in the dense phase resulted in a highly under-expanded jet flow that gradually disappeared with the decrease of the measured pressure in the vessel; larger nozzle sizes lead to lower temperature of the fluid in the vessel during blowdown, with liquid stage releases resulting in a higher temperature drop than gas-phase discharges. As highlighted, experimental studies on CO_2 discharges and accidental releases in the literature are largely based on pipeline systems and high-pressure dense, liquid or gas conditions, with limited studies focusing on liquid CO_2 conditions typical of carbon dioxide shipping for CCUS [22,23]. Moreover, to the best of the authors' knowledge, no study has specifically investigated liquid CO_2 discharges typical of shipping systems under a refrigerated state. While the optimal conditions that future CO_2 shipping projects are still under debate, process safety considerations may well become key decision factors. However, the nature of depressurisation behaviour in liquid CO_2 vessel at conditions typical of sea vessel transportation remains largely unexplored, particularly in relation to the propensity for solid formations in proximity to the triple point that can largely affect safety considerations. Such dearth of knowledge is especially critical when infrastructure concerning large shipping port terminals needs to be implemented, given that liquid CO_2 under refrigerated state needs to be continuously handled throughout the liquefaction plant, storage tanks and loading terminal [19]. Therefore, to address these knowledge gaps, this work presents a novel refrigerated 2.25 L experimental set-up and relative investigation of the leakage behaviour of refrigerated liquid CO_2 at conditions relevant to shipping transportation for CCUS and with variable orifice size. The experimental campaign focuses on fifteen tests related potential shipping conditions affiliated to low-, medium- and high-pressure boundaries in a refrigerated liquid state and scrutinises the discharge process, assessing the propensity for solid blockages on the discharge pipe, pressure and temperature profile as well as inventory solidification in the vessel.

Experimental methodology

The experimental campaign is performed through the set-up represented in Figure 1. The refrigerated test rig features a 2.25 L dome-ended cylindrical pressure vessel with internal diameter of 91.6 mm and 437 mm in length, made of 304L stainless steel. A coil-heat exchanger made of 6 mm copper tubing is soldered around the pressure vessel's surface and enclosed as a cylindrical shell. A vacuum pump is connected to the inlet of the shell and operated to create a layer of thermal insulation around the annulus by removing the air from the shell, thus allowing it to maintain the low-temperature conditions during the conditioning stage of the test. The enclosed vessel as well as the pipework are wrapped in ARMFLEX as thermal insulation material and the system is placed on a platform scale 0 - 150 kg capacity (± 0.05 kg accuracy) - to monitor the mass of inventory in real time throughout the test.

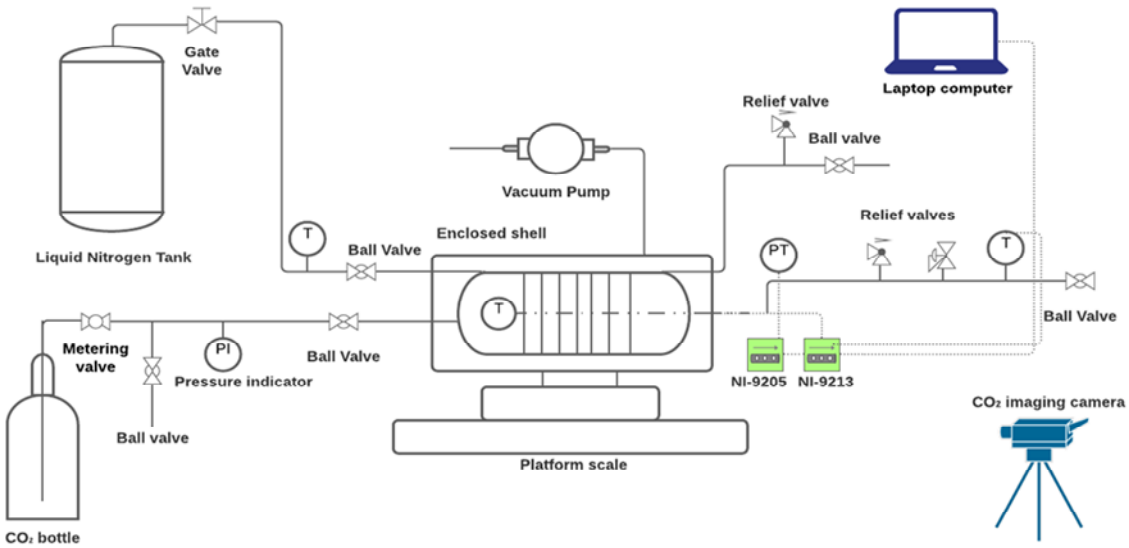

Figure 1: Schematic diagram of the refrigerated experimental set-up

A pressurised liquid nitrogen Dewar (120 L capacity) is connected to the inlet of the coil heat exchanger to supply the refrigerant and cool the liquid CO_2 to the required working temperature. The gate valve fitted at the source of the Dewar allows controlling the flow of liquid nitrogen circulated around the system; upon circulating throughout the coil, the nitrogen is then continuously vented out to atmosphere. A liquid withdrawal bottle is implemented as a CO_2 source (99.8% purity); during the experiments, the bottle withdraws liquid CO_2 and is fitted with a metering valve to

restrict the filling flow and thus control the downstream pressure during conditioning. The discharge line is that of a 6.4 mm outer diameter pipe with a 3.2 mm inner diameter and length of 600 mm. At the end of its length, the pipe is equipped with changeable ball valves with variable orifice diameter. The orifices considered in this work are of 1 mm, 3.2 mm and 4.7 mm. A pressure transmitter (0 - 2.6 MPa measuring range, accuracy ± 0.03 MPa) is installed at a distance of 100 mm downstream the pressure vessel for data acquisition purposes; additionally, a pressure-relief valve and back-pressure regulator are implemented for safety reasons. A k-type thermal well (± 1.5 K) is fitted inside the pressure vessel to monitor its temperature profile during the discharge, and another k-type thermocouple (± 1.5 K) is placed just upstream of the orifice nozzle at a 550 mm length across the discharge pipe. The pressure transmitter and thermocouples are connected to National Instruments 9205 and 9213 modules respectively to enable data acquisition via National Instrument's DAQ Express. Moreover, a FLIR GF343 Optical Gas imaging camera (60 fps) is used to visualise the CO_2 jet flow during the tests. Figure 2 and Figure 3 illustrate the experimental facility and its layout during the tests. The experimental system is designed to operate at a range of pressure and temperature conditions in the CO_2 liquid region spanning from 0.7 MPa and 223 K to 5.7 MPa and 293 K.

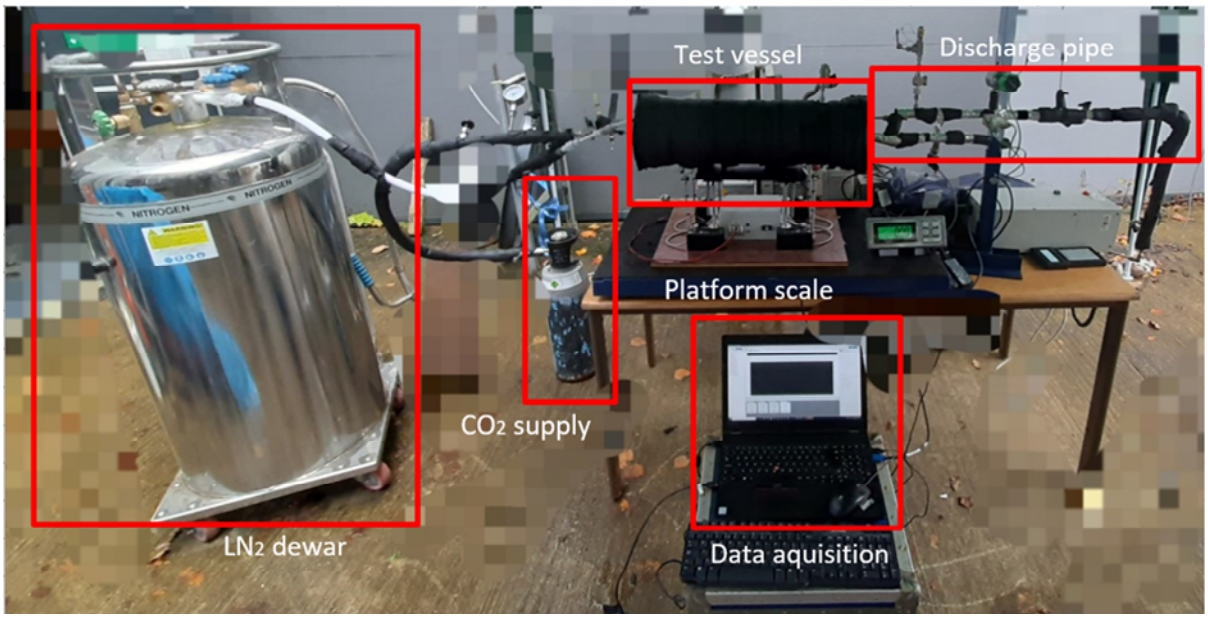

Figure 2: Experimental system for cryogenic liquid CO_2 leakage

Figure 3: left-to-right CO_2 camera acquisition view; enclosure shell and test vessel prior to assembly

Along the length of the discharge pipe section, pressure drop is expected to occur due to momentum and friction loss. Unlike ordinary liquids, Han et al. [22] has highlighted by that the rate of such pressure drop also continues to increase along the length of the discharge pipe. In order to describe this phenomenon, the total pressure drop (∇P_{total}) is presented through a homogeneous model correlation, applicable to both single and two-phase flows above the triple point and given in Equation 1- Equation 4.

$$\nabla P_{total} = \nabla P_{momentum} + \nabla P_{friction} = -\rho_{mixture}\, \mathrm{u}\nabla \mathrm{u} - 2f\, \frac{\rho_{mixture}\, \mathrm{u}^2}{d} \quad \text{Equation 1}$$

$$\mathrm{f} = \frac{0.072}{Re^{0.25}} \quad \text{Equation 2}$$

$$Re = \frac{\rho_{mixture}\, \mathrm{u}d}{\mathrm{\eta}_{mixture}} \quad \text{Equation 3}$$

$$\rho_{mixture} = \frac{\rho_{liquid}\, \rho_{gas}}{\alpha \rho_{liquid} + (1-\alpha)\rho_{gas}};\ \mathrm{\eta}_{mixture} = (1-\alpha)\mathrm{\eta}_{liquid} + \alpha \mathrm{\eta}_{gas} \quad \text{Equation 4}$$

Where u is the flow velocity (m^{-3}), d is the diameter of the pipe (m); Re is the Reynold Number and $\mathrm{\eta}$ is the molecular viscosity (kg m^{-1} s^{-1}). Moreover, ρ denotes the density value in kg m^{-3} and α represents the vapour mass fraction. As demonstrated, the pressure drop is promoted by both momentum change ($\nabla P_{momentum}$) and friction effects ($\nabla P_{friction}$ - emphasised by the Blasius friction factor relation f); when considering discharges scenarios where isenthalpic pressure drop also induces a

change in temperature, it is expected that the density value will also decrease, promoting an acceleration of the flow. In this work, such correlations describe the effect of the pressure drop effects along the discharge pipe, whereby the flow is a mixture of vapour-liquid above the triple point and vapour and solid below the triple point. The temperature change encountered by the fluid when expanded through an insulated (no heat exchanged with the environment) during the discharge through the pipe restriction is described by the Joule Thomson (JT) effect. Its coefficient μ_{JT} thereby reflects the ratio of temperature change to pressure drop at constant enthalpy value, and it is expressed in Equation 5:

$$\mu_{JT} = \left(\frac{\partial \mathrm{T}}{\partial\, \mathrm{P}}\right)_{H} \qquad \text{Equation 5}$$

When the flashing fluid is initially discharged from the vessel, its state at the exit plane is considered to be saturated [34]. Beyond the exit plane, the jet enters in a so-called depressurisation zone, where its pressure progressively equilibrates with the atmosphere; throughout this expansion - assumed to be isenthalpic - the jet eventually equilibrates with the atmosphere and enters a two-phase vapour and solid entrainment zone [34]. An approach proposed by the Energy Institute [34], is to estimate the split vapour and solid fraction at the end of the depressurisation zone; the approach implements conservation principles and assumes that the velocity terms can be neglected. Considering p_1 and h_1 as the initial pressure and enthalpy of the stream and p_2 (= 0.101 MPa) and h_2 as the conditions at the end of the depressurisation zone, the following relationship is thus given in Equation 6.

$$h_1 = h_2 = h_{s,1} + Y_{g,1} h_{sg,1} = h_{s,2} + Y_{g,2} h_{sg,2} \qquad \text{Equation 6}$$

Where Y_g represents the split vapour mass, $h_{sg,1}$ and $h_{sg,2}$ are the difference between solid and gaseous enthalpy at atmospheric pressure; the correlation can thus be rearranged as Equation 7 to give the expected solid mass fraction resulting from the release.

$$Y_s = 1 - \left(\frac{h_2 - h_s}{h_{sg}}\right) \qquad \text{Equation 7}$$

Shafiq et al. [25] derived a correlation to determine the ideal blowdown orifice size to adopt in case of sudden emergency to mitigate the risk of inventory solidification during the unplanned release of CO_2-CH_4 with a ranging CO_2 concentration of 20 – 80 mol% (Equation 8).

$$O = 0.00168 * C_{CO_2} + \frac{14.27 + 0.232 * T_1}{log(4.526 + P_1)} \quad \text{Equation 8}$$

Where O represents the optimum orifice size (mm), C_{CO_2} denotes the molar percentage of CO_2, and T_i and P_i represent the initial temperature (°C) and initial pressure (bar) in the vessel; such correlation is described as a trade-off of maximum orifice size to be selected to avoid solidification of the content whilst also promoting shorter leakage duration as possible. This correlation has been extended to the 100 mol% CO_2 considered in this work to scrutinise its applicability in predicting propensity for inventory solidification at the selected conditions.

Pre-experimental checks

The following experimental procedure was followed rigorously:

1. At the start of the test, the vacuum pump is operated for 30 minutes prior to the injection of carbon dioxide and liquid nitrogen into the apparatus to achieve thermal insulation around the vessel

2. The test vessel is purged with nitrogen gas throughout to eliminate traces of air moisture in the apparatus

3. The liquid nitrogen refrigeration supply is initiated to pre-cool the vessel to 10 K below the intended test temperature

4. Liquid CO_2 in the apparatus is initiated by regulating the metering valve to withdraw at the intended test pressure. The platform scale measurement is switched on and data acquisition is initiated

5. When the target filling of 1.8 kg of CO_2 is achieved as indicated by the platform scale, the supply of carbon dioxide to the system is shut.

6. Test conditions are held for 90 s inside the apparatus. CO_2 camera acquisition is started; the test is therefore initiated by opening the outlet ball valve to begin the discharge

7. The test is considered completed when the system's pressure stabilises to 0.1 MPa (atmospheric pressure)

Operating conditions and intended parameters estimation are summarised in Table 1. Nine refrigerated liquid conditions relevant to potential CO_2 shipping projects for CCUS – affiliated into low, medium and high-pressure conditions - are selected with the aim of investigating the related leakage and discharge behaviour with an orifice size of 3.2 mm. Moreover, three distinct conditions relative to low-, medium- and high-pressure conditions were considered to assess the impact of varying the orifice size (1 mm and 4.7 mm) on the leakage behaviour Ambient temperature measurements are undertaken for all tests and found to be comprised between 283 and 287 K (± 1.5) between all the tests, eliminating its relative dependency. Figure 4 presents an example of the conditioning stage required to achieve experimental conditions.

Table 1: Summary of conditions of discharge tests

Test	Pressure (MPa)	Temperature (K)	Condition	Nozzle size (mm)	Density* (kg/m^3)	Enthalpy* (kJ/kg)
Test 1	0.7	223	Low pressure	3.2	1155	92.7
Test 2	0.83	228		3.2	1136	102.6
Test 3	0.94	225		3.2	1148	96.7
Test 4	1.34	234	Medium pressure	3.2	1114	114.7
Test 5	1.51	242		3.2	1081	131
Test 6	1.67	245		3.2	1068	137.2
Test 7	1.83	249	High pressure	3.2	1051	145.6
Test 8	2.03	254		3.2	1028	156.3
Test 9	2.65	259		3.2	1004	167.2

Test 10	0.7	223	Low Pressure	1	1155	92.7
Test 11	1.54	244	Medium Pressure	1	1072	135.1
Test 12	2.04	254	High Pressure	1	1028	156.3
Test 13	0.7	223	Low Pressure	4.7	1155	92.7
Test 14	1.52	228	Medium Pressure	4.7	1138	102.7
Test 15	2.01	252	High Pressure	4.7	1037	152

properties calculated in NIST REFPROP V9.5

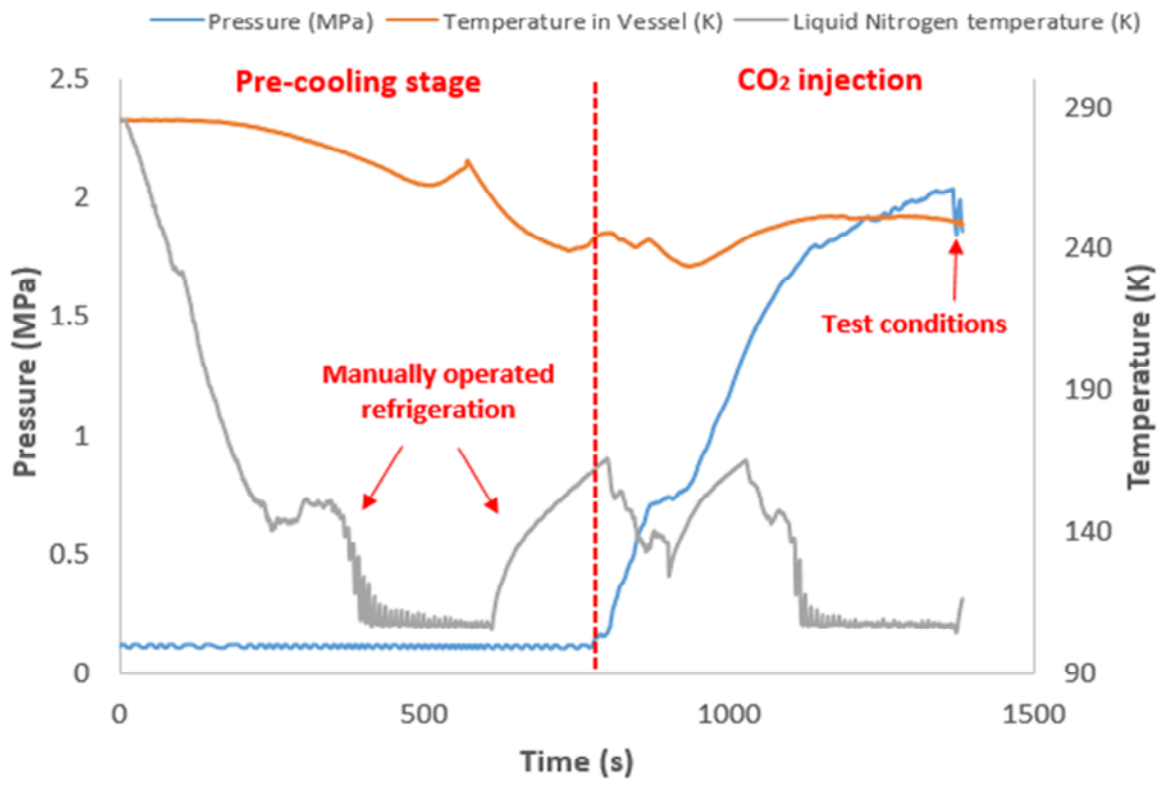

Figure 4: Example of test conditioning profile plot – Test 7 (1.83 MPa, 249 K)

As it is possible to observe in Figure 5, the considered initial CO_2 conditions encompass a wide range in the refrigerated state of liquid CO_2 envelope, exhibiting a

close proximity to the saturation line which are favoured for shipping conditions. The experimental campaign shows the leakage behaviour to be significantly different in relation to the initial inventory condition.

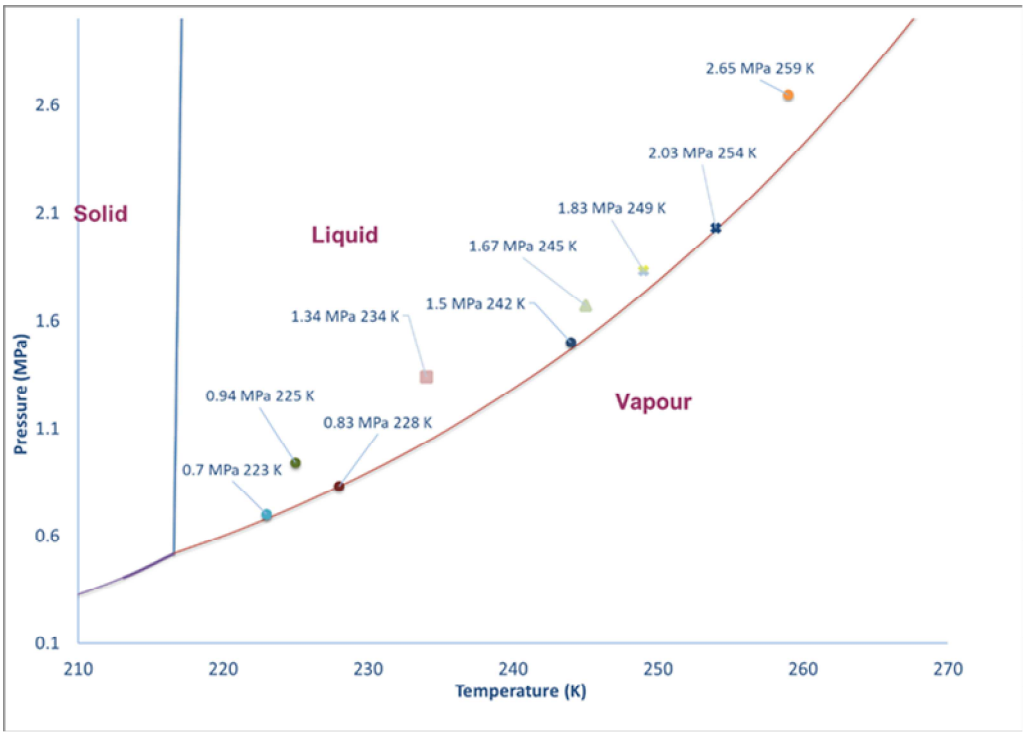

Figure 5: Representation of test conditions on CO_2 phase diagram

Results and Discussion

The typical structure of the initial outflow jet is shown in Figure 6. The jet expands at the exit nozzle, and its structure is characterised by a decompression region of vapour-solid two-phase flow (initial region) and a secondary dispersion region in which the vapour CO_2 equilibrates with the atmosphere whilst entraining air and slumping to the ground [34]. A simplification can allow to state that, provided that downstream (atmospheric) conditions are unvaried, the split vapour mass fraction can be taken to be merely a function of the initial enthalpy so that $Y_g = f(h_1)$ (Equation 6).

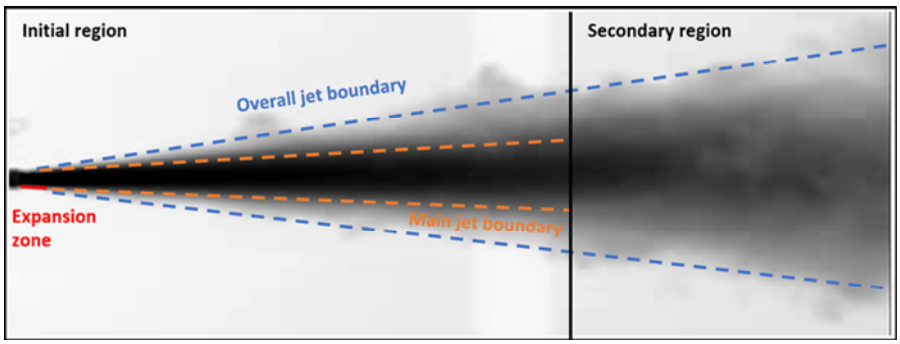

Figure 6: Typical jet structure of CO_2 jet flow; test 8, 3 s

As summarised in Table 1, enthalpy values for the different test conditions are calculated for the different test conditions. This theoretical reconstruction appears to be confirmed in these tests, where the extent of downstream solid fraction produced during the expansion appears to be less remarkable with the increase of initial enthalpy values in the different tests (Figure 7).

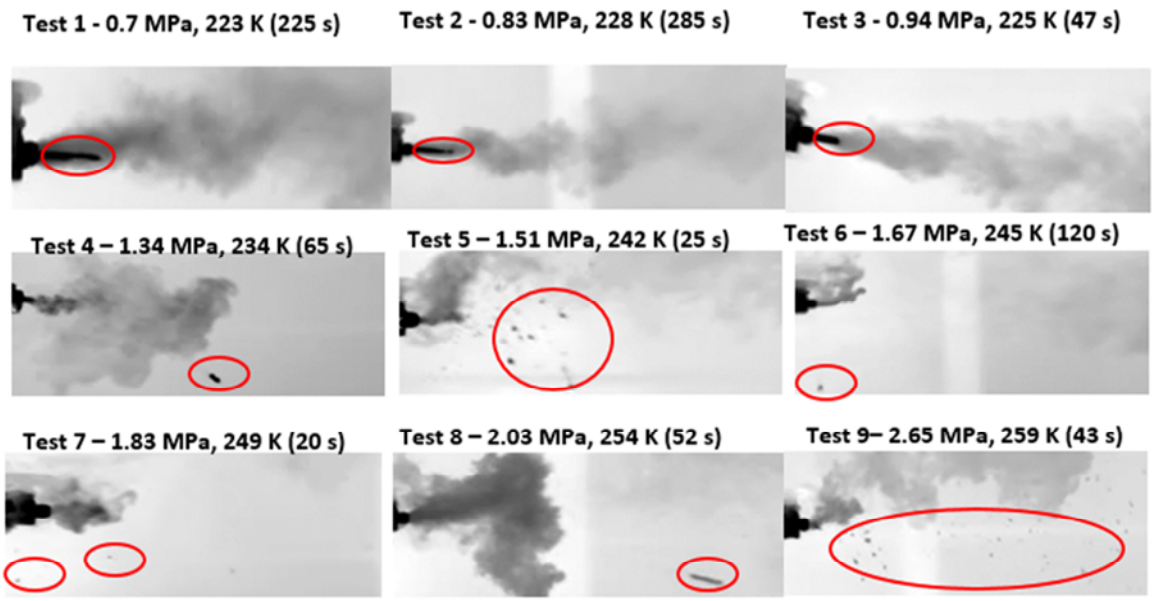

Figure 7: Solid formation in the outflow jet in the experimental tests with 3.2 mm orifice; top-to-bottom: low-pressure, medium-pressure and high-pressure scenarios. Red-circled areas represent solid particles formed in the discharge

Formation of carbon dioxide solids is a complex phenomenon that occurs in several stages; dry-ice particles begin to generate owing to the sudden expansion of liquid carbon dioxide in the aforementioned depressurisation. Size of formed particles and propensity for agglomeration and deposition is found to be accentuated at lower

pressures and smaller margins of initial from sublimation temperature under atmospheric pressure [35,36]. These considerations are reflected in the observation in this work, where the size and quantity of solid particles detected in the outflow cloud is considerably higher in the low-pressure discharges. In case of accidental leak scenarios, it is moreover critical to estimate the instantaneous concentration of CO_2 resulting from the dispersion cloud. CO_2 solid formation thereby represent a critical hazard as during the process of particle sublimation, a localised risk of asphyxiation may arise to personnel located nearby. Pursell [31] provides a simplified equation to estimate the mass of sublimed CO_2 by correlating with presence of diluting air, given as Figure 10;

$$m_{CO_2\,Sub} = km_{air} \qquad \text{Equation 9}$$

Where $m_{CO_2\,Sub}$ represents the mass of sublimed CO_2, k is the linear correlation constant that integrated it with m_{air}, which is the mass of entrained air. Consequently, an empirical correlation was proposed to describe the concentration of CO_2 at any given downstream distance from the leakage source and given as Figure 11.

$$C(x) \approx 5\,\frac{d_e C_0}{x}\left(\frac{\rho_{air}}{\rho_{mixture}}\right) \qquad \text{Equation 10}$$

Where $C(x)$ represents the CO_2 concentration (mol%) at a downstream distance x (m), C_0 is the initial carbon dioxide concentration (mol%) and d_e is the diameter of the source (m) at the atmospheric plane; ρ_{air} and $\rho_{mixture}$ are the air and gas plume density respectively (kg/m^3). As reflected in Figure 6, the resulting expansion of the jet at the exit plane at conditions scrutinised in this work does not show a 'barrel' expansion structure, which indicates a subsonic (M<1) profile at the exit nozzle. This is in contrast with work on higher pressure supercritical and liquid CO_2 releases [31,32] that conversely reportedly show a barrel shock and Mack disk structure that effectively increases the dimension of d_e and thus contributes to a higher CO_2 concentration value at a given downstream distance. Low-pressure streams – possessing a lower initial specific enthalpy value (Table 1) - are associated with a higher mass split fraction of solid phase during isenthalpic expansion of the jet. However, the formed solid plug observed in Figure 7 is found to be suppressing the mass outflow from the vessel in tests 1,2 and 3 since the early stage of the release. Therefore, the risk of asphyxiation

arising from CO_2 concentrations at low-pressure releases appears to be primarily associated with sublimation of localised solid particles expelled during the release.

Impact of initial conditions and orifice size

Upon filling of the inventory and conditioning to the required testing conditions, liquid CO_2 is contained in the pressurised, insulated vessel which enables to keep it in its liquid state. As the tests are initiated and the nozzle orifice is opened to release the CO_2 vapour in the space above the liquid, the content of the vessel begins to discharge to the atmosphere due to the pressure difference between the pressure vessel and the surroundings.

As highlighted in Figure 8 and Figure 9 – which respectively show the pressure and temperature profile of the releases - the considered tests for the low-, medium- and high-pressure transport conditions exhibit a distinctively common discharge behaviour. This observation strengthens the hypothesis that selection of appropriate condition in the refrigerated liquid state is very sensitive to the margin from the triple point. In particular, it is interesting to observe that the modest difference initial conditions exhibited by test 6 (1.67 MPa, 245 K) and test 7 (1.83 MPa, 249 K) leads to a remarkably different leakage time. Alongside the dissimilarities, tests demonstrate common trends - namely the solidification of portion of the inventory that leads to the achievement of ~ 200 K temperature value in the system. As reflected by the distinct leakage duration (Figure 8) reported for each pressure boundary, it appears evident that propensity for solid formation in the discharge pipe is considerably more accentuated at medium pressures (1.34 – 1.67 MPa) compared to high pressure tests (1.83 – 2.65 MPa).

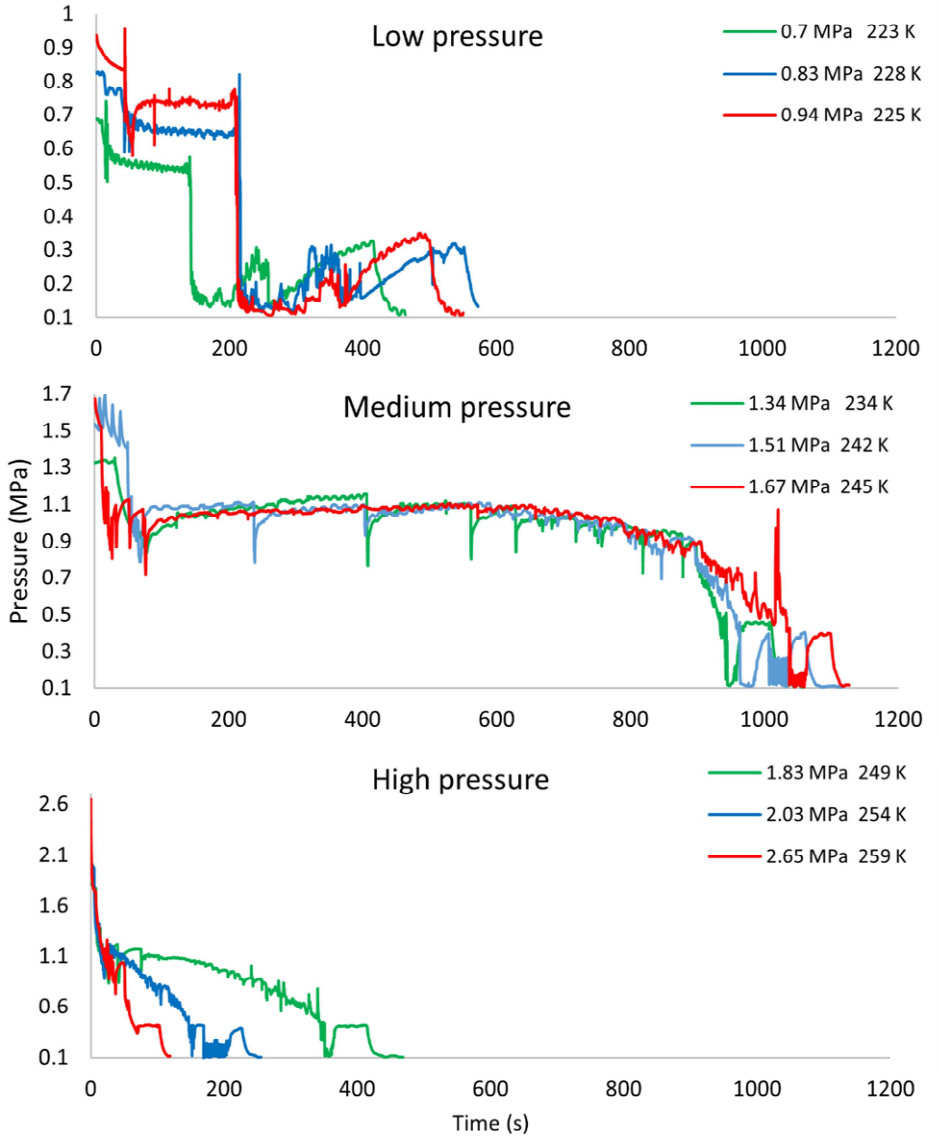

Figure 8: Pressure profile of the experimental tests with 3.2 mm orifice

The low-pressure discharges show an invariable behaviour manifested in several stages (Figure 8 and Figure 9). Test 1, performed at 0.7 MPa and 223 K is hereby considered in more details (Figure 11) to describe the release at low-pressure conditions. The discharge initiates with an initial drop in pressure that could be attributed to the discharge of non-homogeneous gas phase contained in the vessel that brings the pressure to a value of 0.57 MPa [31].

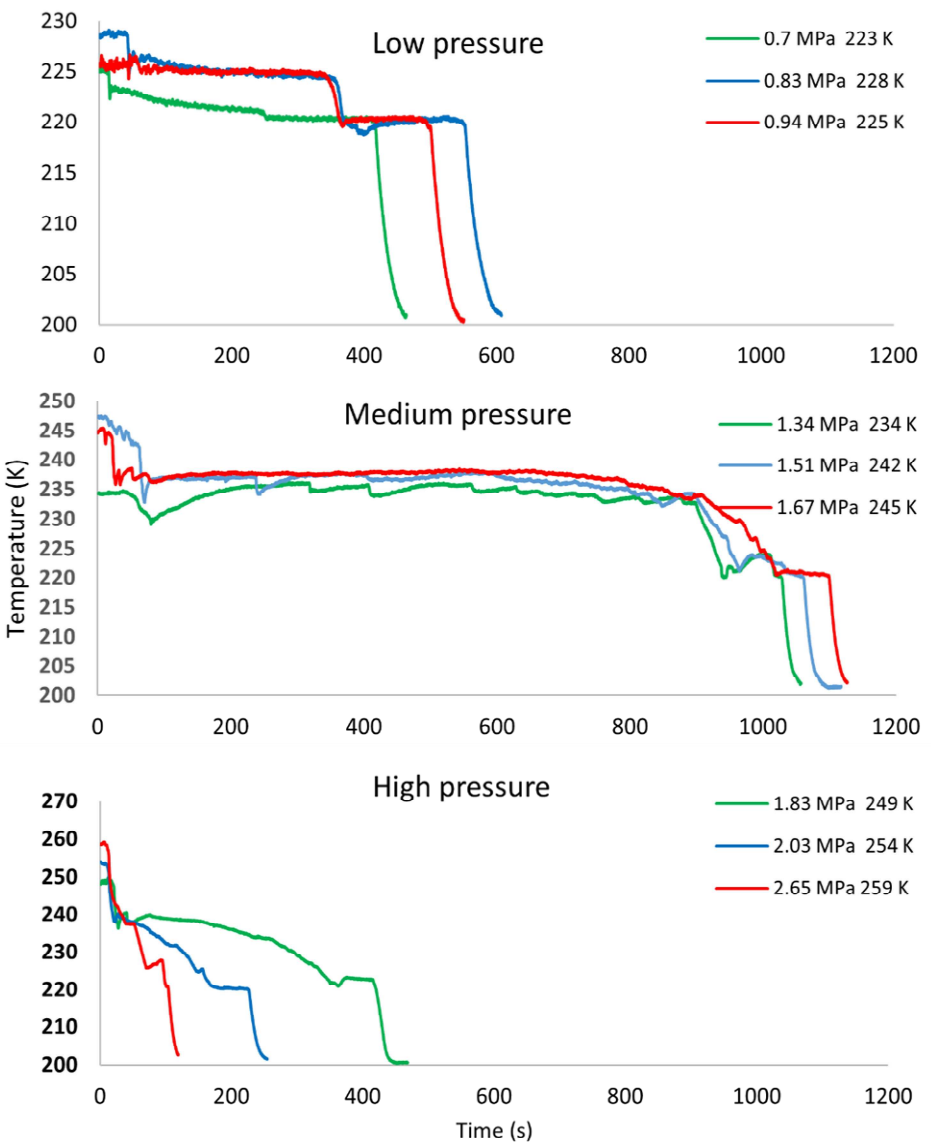

Figure 9: Temperature profile of the experimental tests

At the same time, the process is characterised by the absence of inventory discharge from the early stage of the release in favour of an observed vapour-solid cloud (Figure 10). This is reflected by the presence of a blocked outflow form the pipe whereby no vapour-liquid flow is observed since the early stage of the release, owing to solid accumulation upstream the nozzle (Figure 10). As the fluid leaves the vessel and enters into the pipe section, it undergoes a rapid expansion accompanied by a loss of pressure due to momentum and friction effects; thus, the resulting temperature drop resulting from the Joule-Thomson effect correlated to the pressure drop in the pipe promotes the formation of dry ice particles in the two-phase (vapour-solid) as the flow

condition drops below the tripe point pressure [37]. Indeed, this propensity is favoured by the close proximity of the initial fluid pressure in tests 1, 2 and 3 (0.7 – 0.94 MPa) to the triple point and thus vapour-solid envelope. During this stage, the formed blockages can be considered to be located upstream of the nozzle, as reflected by the absence of flow and measured temperature profile in the discharge pipe. The recorded temperature profile (stage 1), and specifically the 30 K temperature difference between the fluid temperature in the vessel (223 K) and the measured temperature in the discharge line (255 K) confirms this observation (Figure 11). In such scenario the net cooling effect recorded by the thermocouple is conversely given by the accumulated solids sublimating through the pipe and thus progressively cooling the pipework. At the same time, the consistent pressure measurement of ~ 0. 57 MPa demonstrates that the aforementioned solid blockage has generated downstream the pressure transmitter at a distance of >100 mm along the discharge pipe (where the pressure measurement is located).

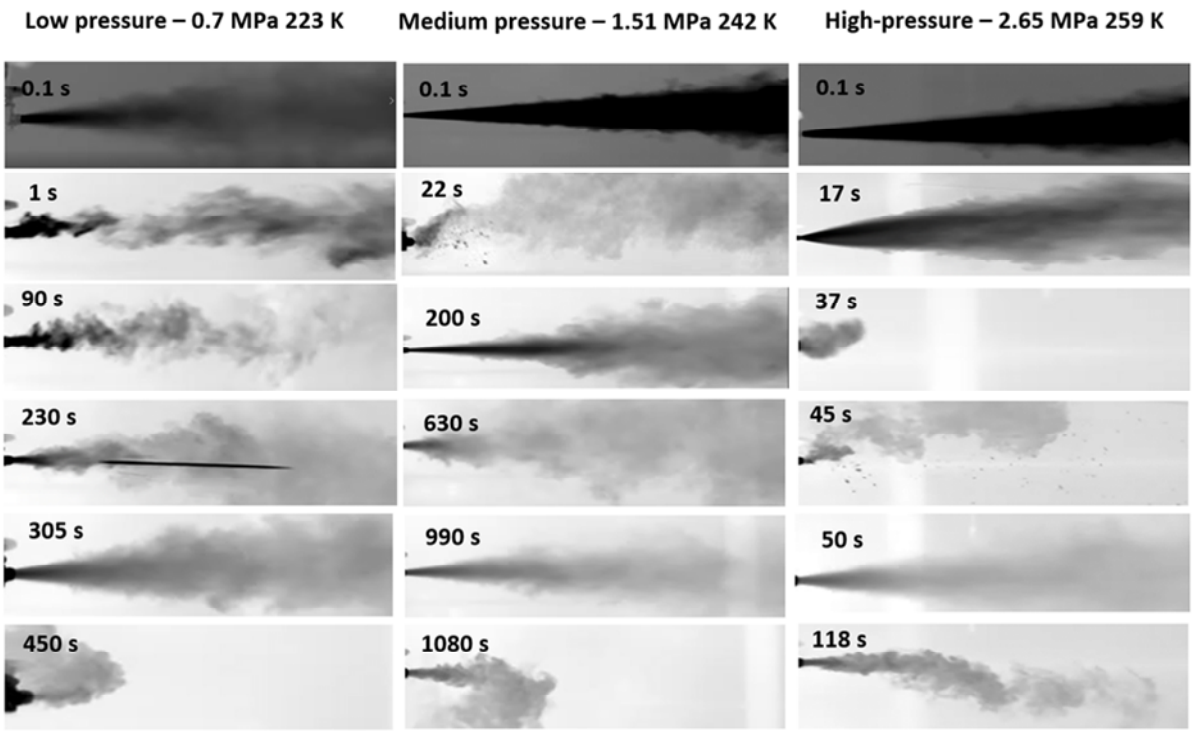

Figure 10: CO_2 jet flow throughout the discharge stages at different pressure conditions

Throughout stage 1, measured pressure shows modest fluctuations likely caused by the intermittent flow vapour-solid flow in the pipe. At 140 s, an abrupt drop in the measured pressure brings the measured value close to atmospheric (0.17 MPa) within 10 s. This trend is common to all performed tests under low-pressure boundaries,

albeit occurring at different pressure conditions, namely at 0.64 MPa in test 2 and at 0.74 MPa in test 3; the steady temperature profile observed in the vessel alongside the fact the such pressure drop occurs at different pressure values in tests 1, 2 and 3 allows to discard correlation of this phenomenon with a phase transition inside the vessel. The observed trend can conversely be attributed to the propagation of dry ice blockages further upstream the pressure transmitter's measurement, potentially at the exit nozzle of the vessel. As found by Teng et al. [36] and Liu et al. [37], pressure and temperature conditions of the stream largely impact the size of formed dry-ice particles: mean particle diameter is found to increase when the margin between initial temperature of CO_2 and sublimation temperature reduces, with a tendency to also reduce with the increase of pressure [36]. Agglomeration and deposition of individual solid particles takes place with particles depositing on the tube wall and entraining in the pipe resulting in a layer formation [37]. Similarly, to the solid generation phenomenon, this process is favoured at lower temperature values and modest velocity of dry-ice jet; this is because low flow velocities promote larger agglomerates sizes due to the larger detachment force applied to the deposition stratification. Therefore, it appears clear that low-pressure conditions scrutinised in this work result in not only in the highest amount of solid generation at the triple point (as per split solid fraction generated during isenthalpic expansion, Equation 7) but they also have the highest propensity for formation of particles with large mean diameter during the complex discharge phenomenon (Figure 7).

The presence of large solid plugs that obstruct the exit nozzle of the vessel is supported by the fact that at 225 s (Figure 7), the recorded video profile shows the ejection of a large solid blockage having the same diameter as the discharge pipe, which can also be observed at 230 s in Figure 10. Such expulsion of dry-ice plug is observed in all low-pressure tests but it does not appear in any of the other tests performed at medium- and high-pressure (Figure 7); this demonstrates that size of formed solid particles and propensity for agglomeration and deposition is noticeably higher at low-pressure conditions. The ejection of the solid plug from the pipe section demonstrates an effect of fluid pressure on the solid blockage, potentially owing to the ongoing vaporisation process-taking place in the vessel (Figure 10). It is noteworthy that previous literature found that active nucleation of liquid CO_2 can delay the phase change form liquid to liquid-vapour state [22], thereby maintaining CO_2 in a metastable

state during the delay, whereby density change is limited. This suggests that vapour-liquid conditions in the vessel may have established before the encountering of this trend.

At 216 s, the pressure begins to progressively increase; this behaviour can be attributed to an increasing pressurisation occurring inside the vessel, and induced by the aforementioned vaporisation process of the inventory. The vaporising CO_2 therefore starts to gradually flow into the pipe and pressure measurement hereby continues to increase until reaching a value of ~0.3 MPa at 240 s. Consequently, the pressure measurement experiences another abrupt drop to 0.15 MPa; conversely to the previously occasion, this phenomenon is hereby accompanied by a temperature reduction inside the vessel, which reaches value of ~220 K that is maintained for 196 s (Figure 11). This trend is also common to the other tests performed at the low temperature envelope, where the pressure drop encountered in stage 2 also occurs alongside a temperature step-change to 220 K - regardless of the initial temperature, as shown in Figure 9. This observation suggests that triple point conditions are established in the system in this stage and the aforementioned pressure drop represents a phase transition of liquid inventory solidifying in the vessel. At this point, the process enters into a new stage (Stage 3) lasting approximately 196 s. Achievement of near-atmospheric pressure in the vessel at the end of stage 2 – prompted by the phase change of inventory promoted at triple point conditions – indeed indicates no vapour pressure left in the system. For this reason, the absence of vapour pressure can maintain the solids generated during the aforementioned expansion promotes a process of sublimation that starts to take place in the vessel in stage 3.

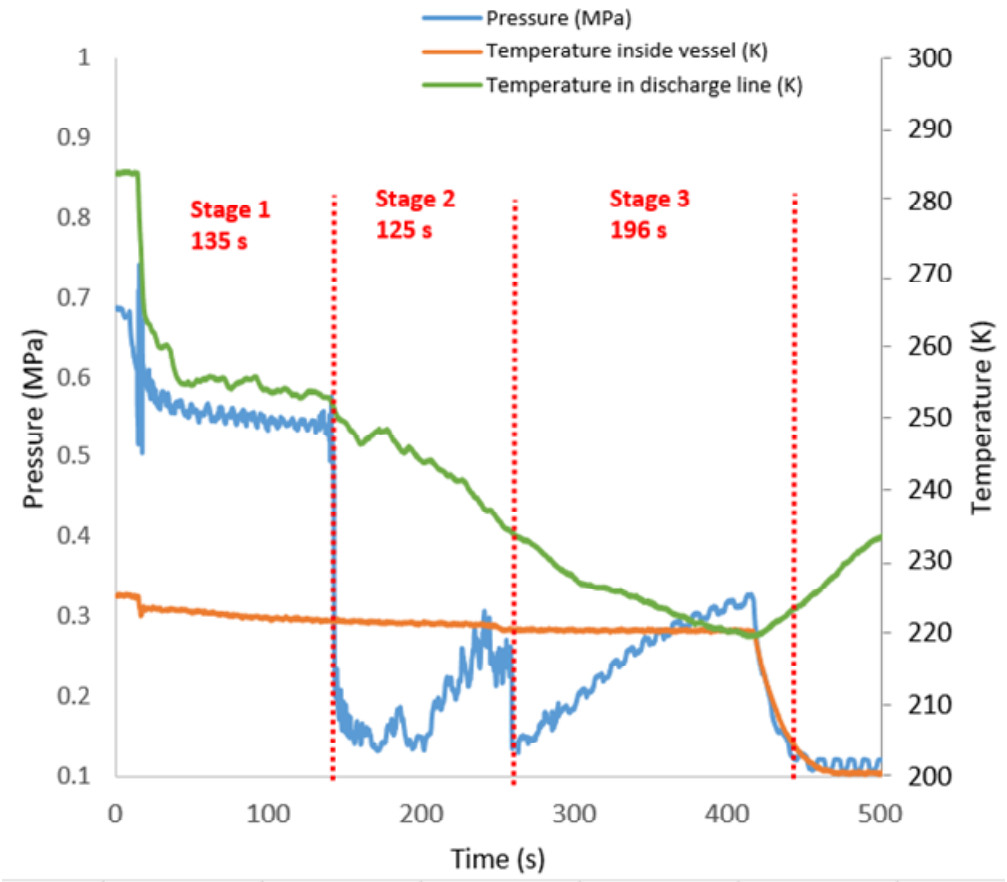

Figure 11: Experimental data of 0.7 MPa and 223 K release (Test 1)

As demonstrated by the tendency for pressure to increase at this stage (from 250 s onwards) – accompanied by absence of signs of blockages highlighted in the camera acquisition profile – it appears that the rate of vaporisation is higher than the outflow rate during this phase. Similarly, to the behaviour encountered throughout stage 2, the pressure increase eventually halts upon reaching the same value of ~0.3 MPa (Figure 11). Following this point, the pressure and temperature profile shows a steady reduction in the vessel – presumably across the sublimation line - whereby CO_2 solid phase under atmospheric pressure is thus generated in the vessel. Medium pressure conditions (tests 4, 5 and 6) also exhibit a distinctively common discharge behaviour as shown in the pressure and temperature profile in Figure 8 and Figure 9. The leakage process (Figure 12) begins with an initial discharge of inventory that lasts for approximately 20 s, promoting a pressure reduction inside the system; the thick jetted cloud observed from 0.1 s (Figure 10) indicates the discharge of saturated inventory, in line with findings from the Energy Institute [34].

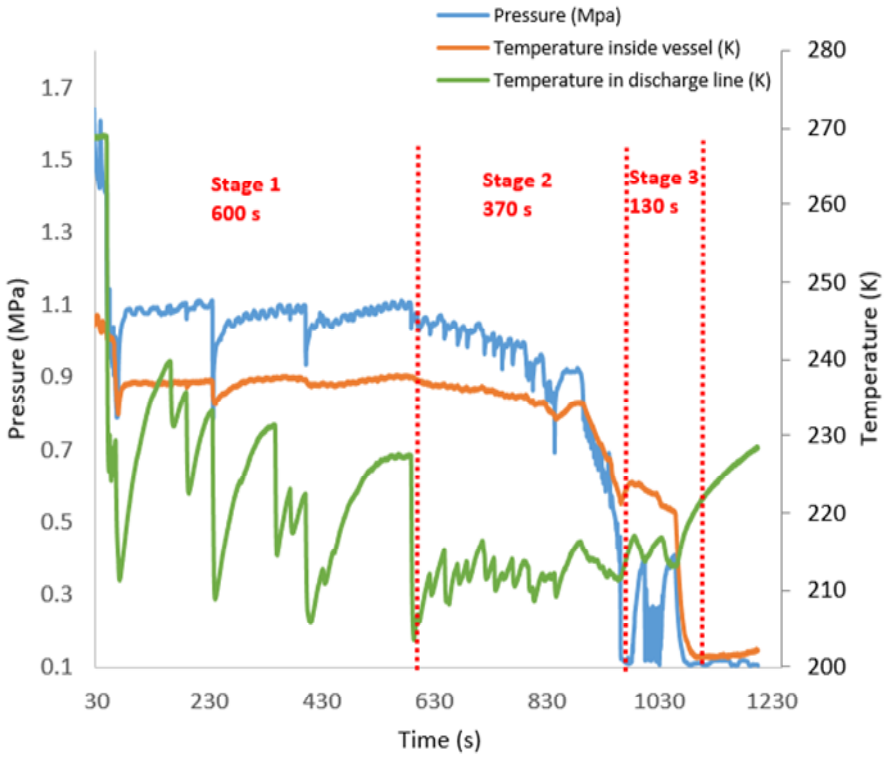

Figure 12: Experimental data of 1.51 MPa and 242 K (Test 4)

It is noteworthy that this initial trend is dissimilar to what encountered in the early release stage at low-pressure conditions, whereby absence of outflow was immediate, implying early formation of solid blockages in the pipe. This difference is due to the fact that the initial conditions of low-pressure tests (0.7 - 0.94 MPa) exhibit a considerably lower margin from the triple point and vapour-solid envelope compared to medium- and high-pressure releases. Eventually, the initial depressurisation stage ends at 22 s, where the system's pressure achieves a value of 1.1 MPa. As in the previous scenario, and owing to the pressure drop effects induced by momentum and friction loss in the pipe, it is possible to assert that the pressure just upstream the exit nozzle drops below the triple point pressure. The flow thus enters and thus enters in a vapour-solid phase at approximately 22 s, as demonstrated by the solid blockage formation that halts the outflow form the system. In particular, the measured temperature of 215 K at 45 s in the discharge pipe reflects the contribution of the resulting Joule Thomson cooling effect correlated with the aforementioned pressure drop, whereby the fluid flow appears to progress in the vapour-solid envelope.

From this point, the pressure and temperature profile in the system enter into a stage that lasts approximately until 600 s (Stage 1), where the profile remains steady except for sporadic discharge resumptions occurring around 230 s and 430 s (Figure 12). Throughout this stage, the suppressed outflow behaviour due to the solid blockage is accompanied by the absence of a significant rate of vaporisation of inventory, which is reflected absence of a pressure accumulation exerted by potential vapour phase that is not able to discharge. The plot of temperature in the discharge line in this stage show considerably large in range and cyclic fluctuations from 240 to 210 K (Figure 12) are reported, strengthening the observation that formation and accumulation of dry-ice solids upstream the exit nozzle was intermittently effecting the discharge of flow. Conversely to the low-pressure scenarios, at medium-pressure condition both the rate of solid formation, dry-ice particle diameter and propensity for agglomeration are found to be lower [36], owing to the higher initial pressure and temperature conditions. As such, it would be intuitive to expect shorter leakage time in the medium pressure scenario as compared to the low-pressure tests, due to the anticipated more modest impact of solid formation in the discharge pipe. The reason why this trend is not observed, and thus why medium pressure releases eventually exhibit considerably higher leakage time is related to sustained solid particles generation in the discharge pipe. As it can be observed in Figure 12, at 230 s the fluid flow temporarily resumes, owing to the ability of the fluid pressure to overcome the formed dry-ice blockages; this is demonstrated by the recorded pressure drop and measured temperature profile in the discharge pipe. However, it also appears evident that such high velocity flow in the vapour-solid phase (temperature in the discharge pipe 210 K) continues to promote more vapour-solid flow and thus solid formation in the pipe (measured temperature value drops again to ~215 K, Figure 12). Due to the thereby reformed solid particles, the discharge halts again, with this trend continuously taking place in a cyclic fashion at ~230 s and 430 s. This process continuously delays the discharge phenomena, resulting in a considerably longer leakage process. This is contrasting with the discharge behaviour displayed by low-pressure scenarios, whereby a complete absence of CO_2 flow is observed in the pipe and a progressive pressure build- up in the vessel due to CO_2 vaporisation effect – contribute to expel the solid. From 600 s (Stage 2), it is possible to observe a continuous resumption of the discharge flow, attributed to the overcoming of the solid blockage in the pipe and reflected in the steadier temperature profile now exhibited in the discharge pipe. It is

particularly interesting to find that the duration of stage 2 appears to be consistent in all of the three medium pressure tests (Figure 8), allowing to assert that within this threshold, combination of initial liquid conditions, flow conditions in the discharge pipe creates a propensity for longer blockages that considerably delay the discharge process. The pressure and temperature within the vessel assume a parabolic decay profile lasting approximately 370 s. When dropping its pressure below the triple point, similarly to what is encountered in the previous set of tests, an accentuated pressure drop brings the measured pressure close to atmospheric values prior to incurring in the pressure and temperature profile described for low-pressure releases (Figure 12). This reflects a common trend for cyclic sublimation and deposition processes.

It is however noteworthy that duration of such stage appears to be different for the different scrutinised conditions: its duration is of 196 s at low-pressure conditions (Figure 11) and 130 s for medium-pressure release (Figure 12). High-pressure releases (test 7, 8 and 9) show a characteristically distinct discharge behaviour as show in Figure 8 and Figure 9. Under these conditions, it can be noticed that leakage duration shows a more remarkable trend of inverse correlation with initial stream pressure (Figure 9). Therefore, having established through the previous paragraphs that formation of CO_2 solids is a significant factor in leakage duration, it is found that selecting a greater margin from the solid envelope demonstrates to be increasingly favourable in minimising the impact of solid formation in the discharge pipe. A characteristic plot of high-pressure releases is presented in Figure 13; as it is possible to observe, an initial discharge (stage 1) lasting approximately 21 s brings the system's pressure to 1.1 MPa.

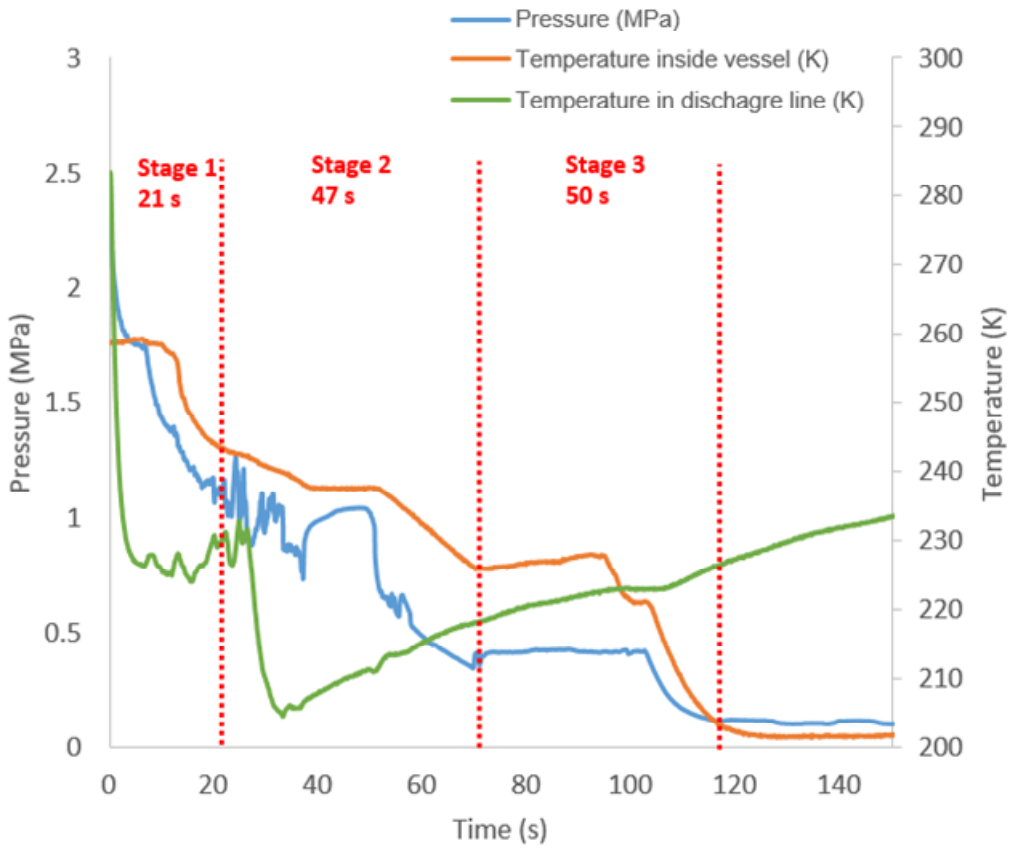

Figure 13: Experimental data of 2.65 MPa and 259 K release (Test 9)

During this stage, the temperature in the discharge pipe also drops significantly, discharging at a ~30 K temperature margin from the temperature measurement in the vessel; similarly, to the medium pressure scenario, this drop in temperature can be ascribed to the Joule-Thomson effect as of the effects as a result of the pressure drop encountered throughout the length of the pipe. The pressure profile begins to fluctuate abruptly due to solid formation in the pipe as the process enters stage 2. During this time, it is noteworthy that the rate of temperature drop in the discharge line also increments significantly; this is potentially owed to the sudden increased temperature drop in the flow promoted by the obstruction of pipe cross surface by means of dry-ice particles. As it is possible to observe in Figure 10, dry-ice formation progressively leads to a blockage that can be seen from 37 to 50 s. This is reflected in the build-up of pressure cause by a continuous evaporation the system that is temporarily unable to fully discharge due to the blockage. At around 50 s, the flow is able to overcome the blockage and the discharge progresses until achieving a plateau (40 s) around the triple point region, which as previously established is associated with the solidification

of part of the inventory. Unlike medium pressure releases, the combination of flow profile through the pipe as well as the quantity and size of solid particles formed during the discharge of the flow does not imply prolonged blockages, demonstrating that the effect of solid formation is considerably more modest under these conditions.

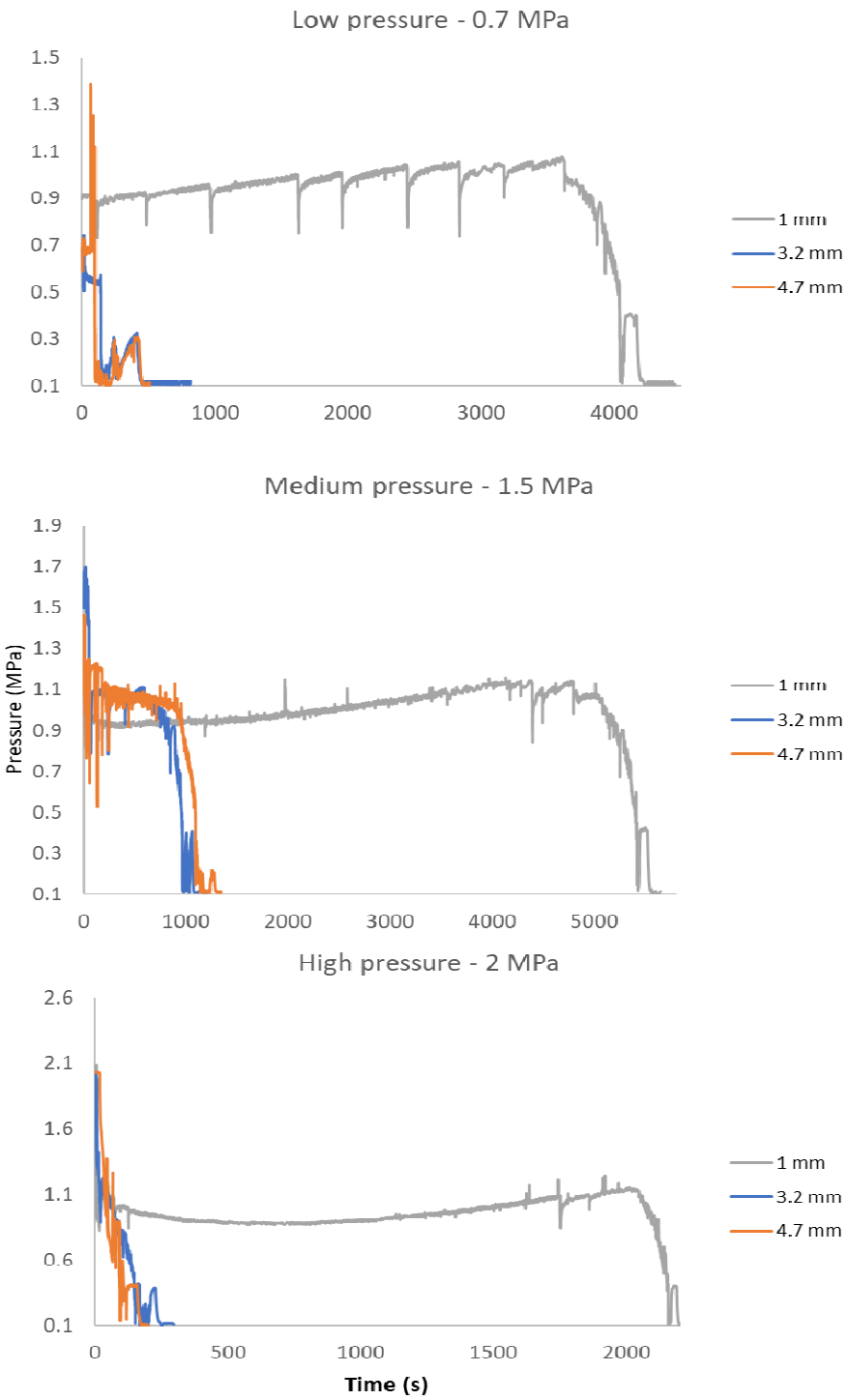

Figure 14: Pressure profile of the discharge under different conditions and orifice sizes

As highlighted in several studies [30,32,33] orifice size has an effect on the depressurisation behaviour of CO_2 under pipeline conditions. This study demonstrates that selection of orifice size can have a profound impact on the discharge under shipping conditions too. Figure 14 shows that a 1 mm orifice results in considerably longer releases in low-, medium- and high-pressure conditions. Thus, it appears evident that leakage from 1 mm orifice generates a propensity for formation of solid CO_2 blockages which halt the discharge process and lead to a progressive increase of pressure in the system. The blockages have variable duration depending on the conditions and the resumption of the leakage process can thereby be potentially attributed to an increase in rate of vaporisation in the system that contributes to expel the blockage from the discharge pipe. In the low-pressure scenario, the flow resumes at 3700 s, after the pressure in the system reaches a value of 1.1 MPa; at 4800 s under medium-pressure conditions upon achieving a value of 1.1 MPa and at approximately 2000 s at 1.1 MPa in the high-pressure scenario. Conversely, the leakage behaviour and duration does not present any significant differences in relation to 3.2 mm and 4.7 mm orifice implying that in that range there is no significant difference in the propensity for solid blockage formation.

Leakage duration and solidification of inventory

The leakage duration and cargo solidification as a result of the discharge process are significantly different in relation to the distinct pressure conditions. As emphasised in Figure 15, releases at medium pressure conditions manifest the highest leakage duration by a significant margin; conversely high-pressure releases show the lowest, with the noticeable trend to reduce with a further increase of pressure. This trend indicates that adoption of an increased margin from the triple point in this range considerably reduces the risk and magnitude of solid formation in the discharge line and vessel system during the release, resulting in overall more linear releases.

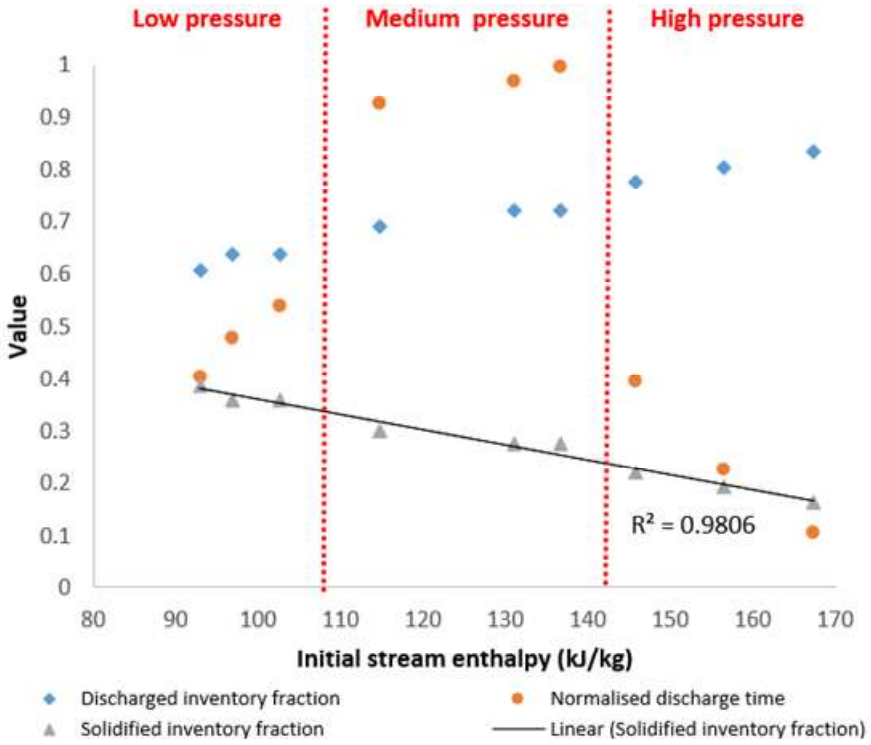

Figure 15: Normalised discharge time and discharged inventory fraction with respect to initial stream's enthalpy at 3.2 mm orifice size

Although low-pressure conditions exhibit a closer proximity to the triple point and thus to the solid envelope, dry-ice formation in the discharge pipe appears to be affecting medium-pressure releases to a greater extent as per duration of the leakage process (Figure 15). As previously explained, this tendency is promoted by the intermittent outflow from the pipe – supposedly in the vapour-solid region - which results in continuous re-formation of solid blockages in a cyclic fashion.

Conversely, the nature of the discharge process concerning low-pressure conditions is such that it results in relatively faster leakage processes albeit with a higher inventory solidification. It is particularly noteworthy that inventory outflow appears to be suppressed from the formation of solid blockages in the pipe form an early stage of the release (Figure 10). The significant outflow of inventory – observed in stage 3 – appears to be limited to a phase transition (sublimation) of solids generated upon achievement of triple point conditions in the vessel. Figure 15 shows a correlation between initial stream's enthalpy, leakage duration and discharged/solidified inventory fraction in all tests. As it is possible to observe, in the low and medium pressure conditions an increase of discharged inventory occurs alongside an increase in discharge time as initial stream's enthalpy increases; in high-pressure releases this

trend is reversed, with discharged amount still increasing with enthalpy, though the normalised leakage time decreases showing a negative correlation.

Table 2: Estimation of optimum orifice size to prevent solidification - Equation 8 - and measured inventory solidification in this work

Conditions	Optimum orifice size (mm)	Orifice size in this work (mm)	Solidified inventory (%)
0.7 MPa, 223 K	1.3	1 – 4.7	36 - 39
1.5 MPa, 242 K	2.5	1 – 4.7	28 -31
2 MPa, 252 K	3.2	1 – 4.7	19

Overall, the increase of the stream's initial specific enthalpy appears to promote a lower level of final inventory solidification in this experimental campaign (Figure 15). Table 2. As it can be observed in Table 2, the discharge process resulted in a variable amount of inventory solidification inside the vessel in the performed tests, ranging from 19% at high pressure to 39% at low pressure conditions. Despite also considering smaller orifice sizes (1 mm) than those indicated by Shafique et al. to avoid solid formation inside the system [25], this work demonstrated that solidification of inventory still occurred in the vessel. Moreover, varying the orifice size did not show any significant difference in rate of inventory solidification at the end of the leakage process. This finding indicates that the proposed correlation does not appear to be suitable for the refrigerated CO_2 conditions considered in this work at 100% mol CO_2 content. This is potentially attributable to the complexity of the phenomenon and the interaction between the liquid, solid and vapour states inside the vessel. Figure 16 shows the plot of the two safety indicators discussed in this work in relation to all experimental tests. Values closer to zero indicate a lower level of inventory solidification at the end of the test (y-axis) and a lower leakage time (x-axis). On the

other hand, a value closer to one denotes a higher level of inventory solidification in the vessel and higher time for the leakage process to complete.

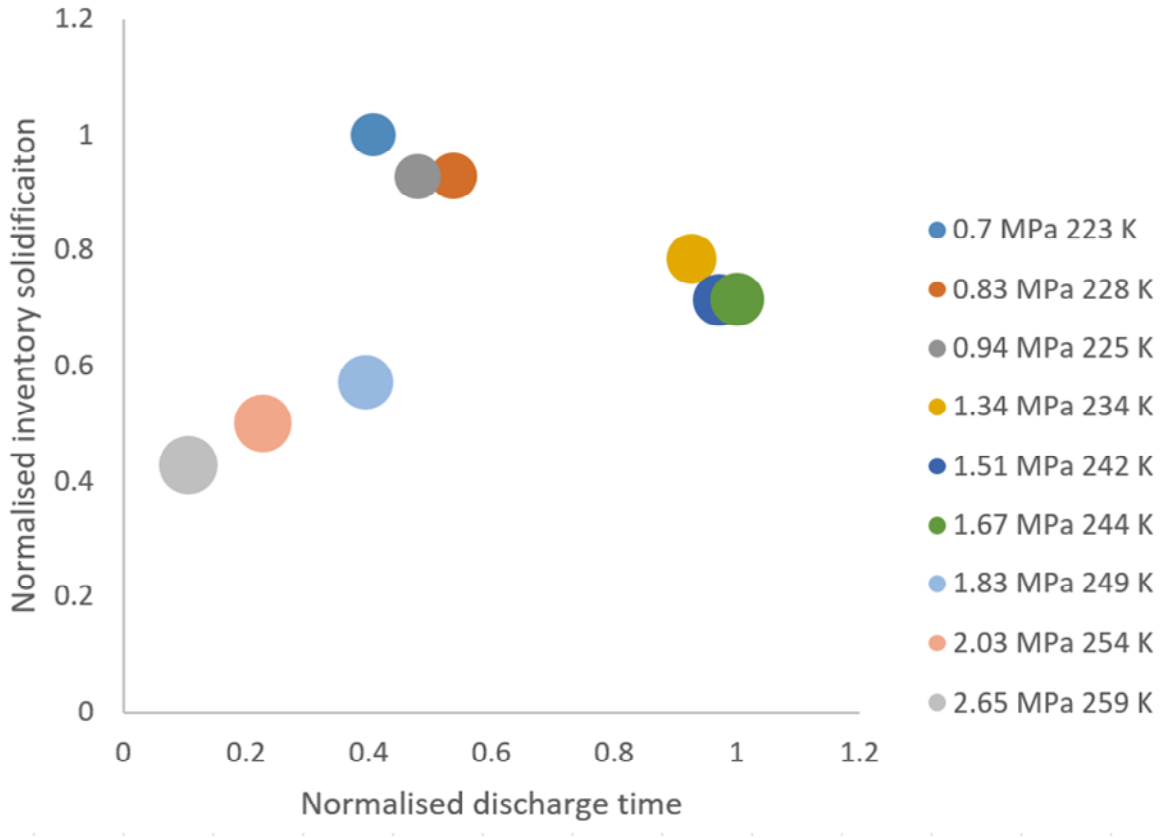

Figure 16 Two-factor safety assessment of liquid CO_2 discharges at shipping conditions (3.2 mm nozzle); values normalised against highest value; bubble area is relative to initial enthalpy of the stream

As shown in Figure 17, normalised discharge time shows a comparable behaviour in relation to both the 3.2 and 4.7 mm orifice size under all conditions. Conversely, leakage duration is significantly higher when 1 mm orifice is considered, with 1.5 MPa liquid conditions (medium pressure) exhibiting the longest duration. Such trend can be attributed to a higher propensity for longer-lasting solid blockages with smaller orifice sizes. In a real CO_2 terminal, liquefied carbon dioxide is expected to be continuously handled between the liquefaction plant, intermediate storage tanks and loading facilities [19]. In assessing the risk for potential loss of containment scenarios, previous studies provided preliminary identification of hazardous occurrences in intermediate storage terminals and sea carriers of a CO_2 port terminal [16,19].

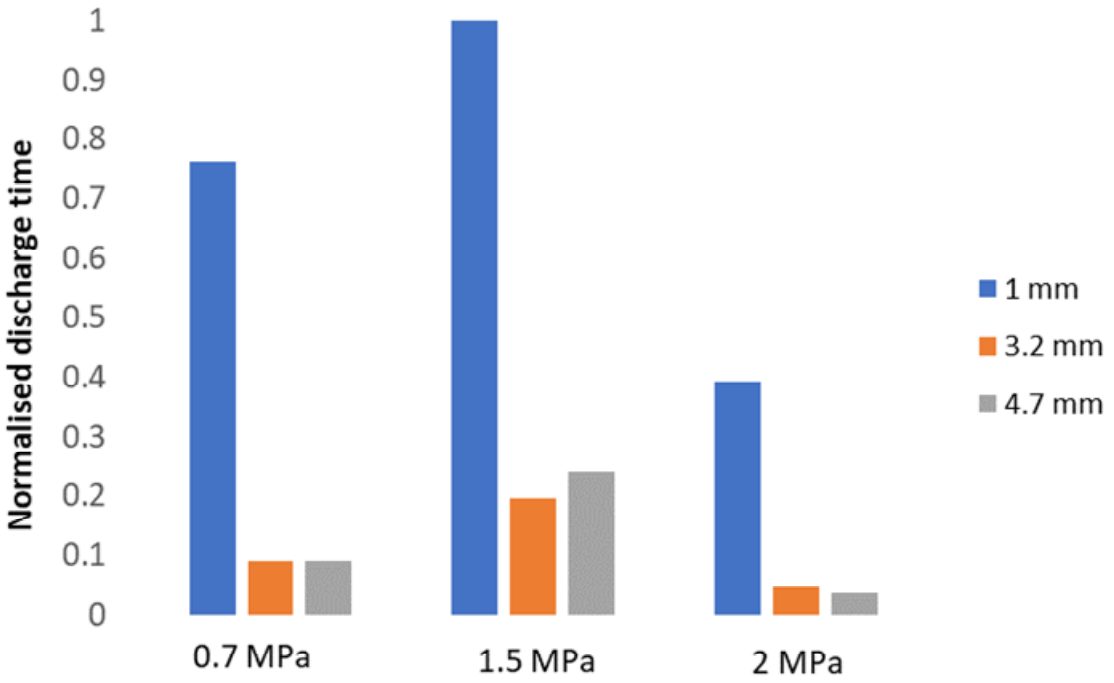

Figure 17: Normalised discharge time of different conditions in relation to variation of orifice diameter

Findings suggested that rupture or leakage from carbon dioxide storage tanks or transmission pipework are among the key hazardous events that need to be considered for safe and reliable operations. As such, scenarios that can pose a risk to plant, people and environment during real operations include overpressure, low pressure, or leakage due to rupture of the tank or pipe section due to mechanical failure. In particular, Koers et al. [19] performed a comprehensive operational safety study on a CO_2 terminal and found that uncontrolled release of inventory is the key hazard to be investigated, with failure modes attributed to corrosion, material failures, equipment failure or incorrect operation. Failure frequency for pressurised storage tanks is higher in a scenario where leakage initiates through a small <10 mm hole (10^{-5} per year) compared to rupture of the storage tank (10^{-7} per year) [19]. This consideration makes this study particularly relevant given its focus on leakages from small orifices. The authors [19] moreover highlight that the risk of uncontrolled release of CO_2 inventory must also be considered for scenarios where liquid CO_2 is transferred from the storage tanks to the loading terminal via piping sections, whereby the failure frequency of pipeline rupture is estimated to be 3×10^{-7} per year. Consequences can be disastrous, resulting in the uncontrolled release of CO_2 inventory which can lead to

dangerous accidents. To reduce such risks, storage tanks and pipelines should be designed and constructed with appropriate materials and suitable thicknesses to accommodate safety design required. In case of overpressure or overcharging, pressure-safety valves and level alarms should be implemented as mitigation measures, alongside emergency shutdown valves that halt the flow of CO_2 [16]. The latter should be fitted as close as possible to storage tanks. Additionally, the installation of low-temperature sensors around the transmissions pipeline can detect CO_2 leakages at an early stage. Moreover, the risk of low-pressure in the tanks – which promotes inventory solidification and blockages – can be reduced by feeding gaseous CO_2 through the boil-off gas return line [16]. In order to implement the appropriate risk-mitigation measures a thorough understanding of the leakage phenomena is required. In particular, this study explored such accidental leakage scenario in relation to different potential shipping conditions which can cool the walls rapidly by the evaporation of liquefied CO_2 and this might cause thermal damage to the infrastructure. This experimental campaign comes with its own set of limitations, such as the inability to assess the representative hazardous distances of the dispersion jet and its interaction with plant, people, and environment; additionally, the considered inventory amounts to a modest quantity, relevant to lab-scale apparatus, rather than that of an industrial storage tank and this is a significant difference between the laboratory environment and real-large scale transport system. Nonetheless, this work provides an understanding of the impact of selecting different CO_2 shipping conditions and orifice size on the leakage behaviour of liquid, refrigerated CO_2. Findings from this paper can moreover be used as benchmark cases for lab experiments and numerical simulations using relevant modelling software packages such as IRATE, DRIFT and PHAST [21]. As it is possible to observe, the plot shows the presence of three distinct clusters, each grouping low-, medium- and high-pressure tests. The high-pressure cluster region exhibits a relatively fast discharge process accompanied by a relatively modest level of inventory solidification inside the vessel. These performance indicators are particularly advantageous to scenarios where the rapid and complete evacuation of cargo inventory is required; for instance, in case of a CO_2 leak in a ship vessel, the defective tank must be emptied as quickly as possible through a jettisoning discharge pipe that is generally larger than the size of the crack in the tank [22]. In such instances, the high-pressure operating conditions investigated in this work appear to be the optimal choice in terms of both duration and maximum discharged amount from

the vessel, and particularly at 2.65 MPa where discharge times and tank solidification have the lowest values.

The low-pressure cluster shows the maximum amount of inventory solidification (0.7 MPa, 223 K) and an intermediate range between the high and medium pressure values when it comes to leakage time. Consequently, the medium pressure cluster is the one that shows the highest discharge times – particularly in the 1.67 MPa scenario – albeit with a relatively more modest fraction of solid formation in the vessel. Indeed, this indicates that the propensity for cyclic formation of solid blockages in case of rupture of circulation pipework is highest under these conditions. This consideration implies relatively longer times for emergency response protocols compared to low- and high-pressure conditions. However, the risk of over-pressurisation cannot be ruled out similarly to pipeline conditions. Overall, both low- and medium-pressure conditions thus appear not to be optimal for an efficient jettisoning process, due to the relatively slower leakage behaviours and higher proportion of content leftover due to solidification. However, in different scenarios involving leaks from storage tanks located at the port terminal, slower discharge processes and lower discharged amount promote the preserving of inventory and allow longer times for emergency response and crack reparation. Low-pressure conditions are recommended when preserving inventory as a result of the leak is preferred, whilst medium pressures represent the better choice if longer leak times are favoured to enable adequate emergency responses. The propensity for pressure increases in the vessel due to pipe blockage is moreover identified as a potential hazard, whereby appropriate implementation of pressure-safety valves is the suggested as a mitigation solution. In such scenario, the demonstrated propensity for large dry-ice plugs to form and progressively propagate inside the pipe at low-pressure conditions requires particular attention in optimal design and selection of suitable location of pressure-safety valves.

Conclusions

In this paper, CO_2 leakage experiments were performed to investigate the discharge behaviour and under refrigerated, liquid CO_2 in a vessel. Parameters such as pressure, temperature of the fluid within the vessel and in the discharge line, and outflow jet dispersion were acquired to experimentally analyse releases of liquid CO_2 at conditions relevant to the shipping chain. The following conclusions are therefore formulated through this study:

- A distinctively common release behaviour is observed relative to initial condition boundaries - namely low (0.7 - 0.94 MPa), medium (1.34 - 1.67 MPa) and high pressure (1.83 - 2.65 MPa) – demonstrating that selection of appropriate fluid conditions in the refrigerated liquid state is highly sensitive to the proximity to the triple point

- High pressure conditions (1.83 – 2.65 MPa, tests 7,8,9) showed more linear and overall smoother discharges, owing to a lower extent of solid formation in the system; this trend further accentuates with the increase of initial pressure and temperature conditions, demonstrated the increased benefits of operating at a further margin form the triple point

- A two-factor safety assessment accounting for both inventory solidification and duration of the leakage process revealed that selection of higher-pressure conditions (1.83 – 2.65 MPa) is optimal when low rate of inventory solidification and faster discharge processes are desired

- Medium pressure releases (1.34 – 1.67 MPa) show the highest leakage duration - attributed to the cyclic reformation of solid particles from the vapour-solid flow profile in the discharge pipe - and a middle ground value of inventory solidification. Such conditions therefore favour scenarios where allowing for longer response times to implement mitigation measures is prioritised

- Low pressures discharges (0.7 – 0.94 MPa) exhibit the largest fraction of inventory solidification alongside an intermediate value of leakage duration; therefore, these conditions are to be considered advantageous when preservation of inventory is the main priority.

- Reduction of orifice size from 3.2 - 4.7 mm to 1 mm demonstrated significant impact on leakage duration under low-, medium- and high-pressure conditions; conversely, variation of orifice size did not show any impact on rate of inventory solidification.

Findings from this work can be used as an overview to the safety considerations concerning different potential shipping conditions, and thus contributing to the formulation of protocols to be adopted in future sea vessel transport projects. Future

work will investigate the leakage behaviour of CO_2 in binary and tertiary mixtures with presence of contaminants such as Ar, CO, H_2 and N_2 which can be found in the CCUS chain.

Acknowledgements

The authors would like to acknowledge for financial support of the project form the Engineering and Physical Sciences Research Council (EPSRC Grant No: EP/N029429/1) and Cranfield Doctoral Training Partnership. FLIR Systems is also acknowledged for granting use of the GF343 Optical Gas Imaging Camera implemented in this work.

References

[1] ZEP. Role of CCUS in a below 2 degrees scenario 2018:1–30. https://zeroemissionsplatform.eu/wp-content/uploads/ZEP-Role-of-CCUS-in-below-2c-report.pdf

[2] Bui M, Adjiman CS, Bardow A, Anthony EJ, Boston A, Brown S, et al. Carbon capture and storage (CCS): The way forward. Energy Environ Sci 2018;11:1062–176.

[3] DNV. Report Activity 5: CO_2 transport. 2012. Report No./DNV Reg No.: 2012-0076/ 13REPT4-2 - Det Norske Veritas.

[4] Barrio M, Aspelund A, Weydahl T, Sandvik TE, Wongraven LR, Krogstad H, et al. Ship-based transport of CO_2. Greenh. Gas Control Technol., 2005; 7:1655–60.

[5] Decarre S, Berthiaud J, Butin N, Guillaume-Combecave JL. CO_2 maritime transportation. Int J Greenh Gas Control 2010;4:857–64.

[6] Hasan MMF, First EL, Boukouvala F, Floudas CA. A multi-scale framework for CO_2 capture, utilization, and sequestration: CCUS and CCU. Comput Chem Eng 2015; 81:2–21.

[7] Roussanaly S, Hognes ES, Jakobsen JP. Multi-criteria analysis of two CO_2 transport technologies. Energy Procedia 2013; 37:2981–8.

[8] Fimbres Weihs GA, Kumar K, Wiley DE. Understanding the Economic Feasibility of Ship Transport of CO_2 within the CCS Chain. Energy Procedia 2014; 63:2630–7.

[9] ZEP. The Costs of CO_2 Transport Post-demonstration CCS in the EU; 2011. European Technology Platform for Zero Emission Fossil Fuel Power Plants, Zero Emissions Platform. Available at https://www.globalccsinstitute.com/resources/publications-reports-research/the-costs-of-co2-transport-post-demonstration-ccs-in-the-eu/

[10] Element Energy. CCS deployment at dispersed industrial sites; 2020. Department for Business Energy and Industrial Strategy; Research paper number 2020/030.

[11] Neele F, De Kler R, Nienoord M, Brownsort P, Koornneef J, Belfroid S, et al. CO_2 Transport by Ship: the way forward in Europe. Energy Procedia 2017; 114:6824–34.

[12] Al Baroudi H, Awoyomi A, Patchigolla K, Jonnalagadda K, Anthony EJ. A review of large-scale CO_2 shipping and marine emissions management for carbon capture, utilisation and storage. Appl Energy 2021;287:116510. https://doi.org/10.1016/j.apenergy.2021.116510

[13] IEAGHG. The Status and Challenges of CO_2 Shipping Infrastructures. 2020; IEAGHG Technical Report 2020-10.

[14] Element Energy, TNO, Engineering Brevik, SINTEF, Polarkonsult. Shipping UK Cost Estimation Study; 2018. Available at: https://assets.publishing.service.gov.uk/government/uploads/system/uploads/attachment_data/file/761762/BEIS_Shipping_CO2.pdf .

[15] Ministry of Petroleum and Energy N, Gassco, Gassnova. Feasibility study for full-scale CCS in Norway. 2016. Available at: https://ccsnorway.com/wp-content/uploads/sites/6/2019/09/feasibilitystudy_fullscale_ccs_norway_2016.pdf

[16] Noh H, Kang K, Huh C, Kang SG, Seo Y. Identification of potential hazardous events of unloading system and CO_2 storage tanks of an intermediate storage terminal for the Korea clean carbon storage project 2025. Int J Saf Secur Eng 2018; 8:258–65.

[17] Patchigolla K, Oakey JE, Anthony EJ. Understanding dense phase CO_2 corrosion problems. Energy Procedia. 2014; 63:2493–9.

[18] Patchigolla K, Oakey JE. Design Overview of High-Pressure Dense Phase CO_2 Pipeline Transport in Flow Mode. Energy Procedia. 2013; 37:3123–30.

[19] Koers P, Looij M de. Final Public Report Safety Study for Liquid Logistics Shipping Concept. 2011; https://www.globalccsinstitute.com/archive/hub/publications/19011/co2-liquid-logistics-shipping-concept-llsc-overall-supply-chain-optimization.pdf

[20] Energy Institute. Hazard analysis for offshore carbon capture platforms and offshore pipelines. 2013; https://www.globalccsinstitute.com/archive/hub/publications/115563/hazard-analysis-offshore-platforms-offshore-pipelines.pdf

[21] Harper P, Wilday J, Bilio M. Assessment of the major hazard potential of carbon dioxide (CO_2). Health and Safety Executive. 2015.

[22] Han SH, Chang D, Kim J, Chang W. Experimental investigation of the flow characteristics of jettisoning in a CO_2 carrier. Process Saf Environ Prot 2013; 92:60–9.

[23] Han SH, Chang D. Dispersion analysis of a massive CO_2 release from a CO_2 carrier. Int J Greenh Gas Control 2014; 21:72–81.

[24] Shafiq U, Shariff AM, Babar M, Ali A. A study on blowdown of pressurized vessel containing $CO_2/N_2/H_2S$ at cryogenic conditions. IOP Conf Ser Mater Sci Eng 2018;458.

[25] Shafiq U, Shariff AM, Babar M, Azeem B, Ali A. Study of dry ice formation during blowdown of CO_2 -CH_4 from cryogenic distillation column. J Loss Prev Process Ind 2020; 64:104073.

[26] Liu Z, Zhao Y, Ren T, Qian X, Zhou Y. Experimental study of the flow characteristics and impact of dense-phase CO_2 jet releases. Process Saf Environ Prot 2018;116:208–18.

[27] Gu S, Li Y, Teng L, Wang C, Hu Q, Zhang D, et al. An experimental study on the flow characteristics during the leakage of high pressure CO_2 pipelines. Process Saf Environ Prot 2019;125:92–101.

[28] Mocellin P, Vianello C, Salzano E, Maschio G. Pressurized CO_2 releases in the framework of carbon sequestration and enhanced oil recovery safety analysis : Experiments and model. Process Saf Environ Prot 2018;116:433–49.

[29] Hébrard J, Jamois D, Proust C, Spruijt M, Hulsbosch-dam CEC. Medium scale CO_2 releases. Energy Procedia 2016;86:479–88.

[30] Hulsbosch-Dam C, de Jong A , Zevenbergen J, Peeters R. Vertical CO_2 release experiments from a 1 liter high pressure vessel. Energy Procedia, vol. 37, 2013, 4712–23.

[31] Pursell M. Experimental investigation of high-pressure liquid CO_2 release behaviour. Inst Chem Eng Symp Ser 2012:164–71.

[32] Xie Q, Tu R, Jiang X, Li K, Zhou X. The leakage behavior of supercritical CO_2 flow in an experimental pipeline system. Appl Energy 2014; 130:574–80.

[33] Tian G, Zhou Y, Huang Y, Wang J, Wang Y. Experimental study of accidental release behavior of high-pressurized CO_2 vessel. Process Saf Environ Prot 2021; 145:83–93.

[34] Energy Institute. Hazard analysis for offshore carbon capture platforms and offshore pipelines. September 2013; https://www.globalccsinstitute.com/archive/hub/publications/115563/hazard-analysis-offshore-platforms-offshore-pipelines.pdf

[35] Hulsbosch-dam CEC, Spruijt MPN, Necci A, Cozzani V. Assessment of particle size distribution in CO_2 accidental releases. J Loss Prev Process Ind 2012; 25:254–62.

[36] Teng L, Li Y, Zhang D, Ye X, Gu S, Wang C, et al. Evolution and Size Distribution of Solid CO_2 Particles in Supercritical CO_2 Releases 2018. Ind. Eng. Chem. Res. 2018, 57, 7655 - 7663

[37] Liu Y, Calvert G, Hare C, Ghadiri M, Matsusaka S. Size measurement of dry ice particles produced from liquid carbon dioxide. J Aerosol Sci 2012; 48:1–9.